Microfoam formation in a capillary

Spiros Kotopoulis, Michiel Postema

Microfoam formation in a capillary

Spiros Kotopoulis, Michiel Postema [1]

Emmy-Noether Group
Institute of Medical Engineering
Department of Electrical Engineering and Information Technology
Ruhr-Universität Bochum
D–44780 Bochum
Germany

Department of Engineering
The University of Hull
Kingston upon Hull
HU6 7RX
United Kingdom

---

[1] Corresponding author. Address: Emmy-Noether Group, Institute of Medical Engineering, Department of Electrical Engineering and Information Technology, Ruhr-Universität Bochum, D–44780 Bochum, Germany.
Telephone: +49 234 3226504. E-mail: michiel.postema@rub.de

Preprint submitted to Elsevier *25 September 2009*

Abstract

The ultrasound-induced formation of bubble clusters may be of interest as a therapeutic means. If the clusters behave as one entity, *i.e.*, one mega-bubble, its ultrasonic manipulation towards a boundary is straightforward and quick. If the clusters can be forced to accumulate to a microfoam, entire vessels might be blocked on purpose using an ultrasound contrast agent and a sound source.

In this paper, we analyse how ultrasound contrast agent clusters are formed in a capillary and what happens to the clusters if sonication is continued, using continuous driving frequencies in the range 1–10 MHz. Furthermore, we show high-speed camera footage of microbubble clustering phenomena.

We observed the following stages of microfoam formation within a dense population of microbubbles before ultrasound arrival. After the sonication started, contrast microbubbles collided, forming small clusters, owing to secondary radiation forces. These clusters coalesced within the space of a quarter of the ultrasonic wavelength, owing to primary radiation forces. The resulting microfoams translated in the direction of the ultrasound field, hitting the capillary wall, also owing to primary radiation forces.

We have demonstrated that as soon as the bubble clusters are formed and as long as they are in the sound field, they behave as one entity. At our acoustic settings, it takes seconds to force the bubble clusters to positions approximately a quarter wavelength apart. It also just takes seconds to drive the clusters towards the capillary wall.

Subjecting an ultrasound contrast agent of given concentration to a continuous low-amplitude signal makes it cluster to a microfoam of known position and known size, allowing for sonic manipulation.

Key words: Capillary blocking, Embolisation, Microfoam, Radiation forces, Ultrasound contrast agent
PACS: 43.25.Yw; 47.55.df; 87.50.yt

1 Introduction

Ultrasound contrast agents are used in diagnostic imaging. They consist of microscopically small bubbles containing slowly diffusing gas encapsulated by biodegradable shells. When inserted in the blood stream, these bubbles oscillate upon ultrasonic sonication, thereby creating detectable ultrasound themselves. A brief overview of the most common ultrasound contrast agents has been presented in [1]. It follows that albumin and lipids are currently the most common bubble encapsulation materials. Because of the proven feasibility to attach therapeutic compounds to albumin and lipids, therapeutic applications of contrast agents have become of interest [2–5]. It is desirable that the therapeutic load of any such contrast agent is released close to the vessel wall. Therefore, pushing bubbles towards boundaries by means of primary radiation forces has been studied [6]. Both primary and secondary radiation forces resulting from oscillating bubbles, may cause the repulsion or mutual attraction, and eventual collision and coalescence, of contrast agent bubbles. This phenomenon has been less studied.

From the therapeutic point of view, the formation of bubble clusters may be of interest. If the clusters behave as one entity, *i.e.*, one mega-bubble, its ultrasonic manipulation towards a boundary is fairly straightforward and quick. If the clusters can be forced to accumulate to a microfoam, entire vessels might be blocked on purpose using an ultrasound contrast agent and a sound source.

In this paper, we analyse how ultrasound contrast agent clusters are formed and what happens to the clusters if sonication is continued. Furthermore, we show high-speed camera footage of microbubble clustering phenomena and discuss the therapeutic consequences of our findings.

2 Theory

A brief overview of theory on radiation forces and ultrasound contrast agent has been given in [7]. Bubble translation in the direction of the sound field is caused by a primary radiation force resulting from a pressure gradient across the bubble surface. The translation is maximal in contraction phase. The velocity v of a bubble in a steady fluid subjected to an ultrasound field can be calculated using [8]:

$$F_\mathrm{r} + F_\mathrm{d} - \frac{\mathrm{d}(mv)}{\mathrm{d}t} \approx 0, \tag{1}$$

where F_r is the primary radiation force, F_d is the drag force, $m = \frac{2}{3}\pi\rho R_0^3$ is the added mass of the translating bubble, equivalent to half the mass of the displaced surrounding fluid, in which R_0 is the equilibrium bubble radius and ρ is the density of the surrounding fluid. Averaging over one acoustic cycle, the primary radiation force is given by [8,9]:

$$F_\mathrm{r} = \frac{p_\mathrm{a}^2 R_0}{\rho\, c\, f} \frac{\delta\left(\frac{f_0}{f}\right)}{\left[\left(\frac{f_0}{f}\right)^2 - 1\right]^2 + \left[\delta\left(\frac{f_0}{f}\right)\right]^2}, \tag{2}$$

where c is the speed of sound, p_a is the peak rarefactional acoustic pressure, δ is the dimensionless total damping coefficient [10], f is the driving frequency, and f_0 is the bubble resonance frequency [10]. The drag force is given by [9,11]:

$$F_\mathrm{d} = -\frac{\pi\eta}{4} C_\mathrm{d}\, \mathrm{Re}\, R_0\, v(t), \tag{3}$$

where η is the shear (dynamic) viscosity of the fluid, $\mathrm{Re} = \frac{2\rho R_0}{\eta}\,|v(t)|$ is the Reynolds number, and

$$C_\mathrm{d} = \frac{24}{\mathrm{Re}}(1 + 0.15\,\mathrm{Re}^{0.687}) \tag{4}$$

is the drag coefficient of a contaminated system [12], such as a contrast agent.

Combining equations (1)–(3) and integrating over dt gives the following expression for the average velocity of a bubble:

$$v = \frac{4\,p_\mathrm{a}^2}{\rho\,c\,f\,\eta\,C_\mathrm{d}\mathrm{Re}} \frac{\delta\left(\dfrac{f_0}{f}\right)}{\left[\left(\dfrac{f_0}{f}\right)^2 - 1\right]^2 + \left[\delta\left(\dfrac{f_0}{f}\right)\right]^2} \left[1 - e^{\left(-\frac{3\,\eta\,C_\mathrm{d}\,\mathrm{Re}}{8\,\rho\,R_0^2}t\right)}\right]. \tag{5}$$

Secondary radiation forces, resulting from oscillating bubbles under sonication, may cause the mutual attraction and subsequent coalescence of contrast microbubbles. Two bubbles that oscillate in phase approach each other, whereas two bubbles that oscillate out of phase recede from each other [13,14]. At low acoustic amplitudes, the phase angle difference ϕ between excursion of the oscillating bubble and the incident sound field is given by [13,14]:

$$\phi = \pi + \arctan\left(\frac{\delta\left(\dfrac{f}{f_0}\right)}{1 - \left(\dfrac{f}{f_0}\right)^2}\right). \tag{6}$$

The presence of an encapsulating shell increases the damping coefficient by a term δ_s [15]

$$\delta_\mathrm{s} = \frac{S_\mathrm{f}}{2\pi\,m\,f_0}, \tag{7}$$

and increases the squared resonance frequency f_0^2 by a term f_s^2 [15]

$$f_\mathrm{s}^2 = \frac{\chi}{2\pi R_0^3 \rho}, \tag{8}$$

where S_f is the shell friction [15] and χ is the shell stiffness parameter [14,15]

$$\chi = \frac{E\epsilon}{1 - v}, \tag{9}$$

in which E is Youngs modulus, ϵ is the shell thickness, and v is the Poisson ratio.

The mean approach velocity u of two identical bubbles is given by [8]:

$$u = \frac{\mathrm{d}d}{\mathrm{d}t} = -\frac{(2\pi\,f\,p_\mathrm{a})^2}{27\,\eta}\rho\,\kappa^2\frac{R_0^5}{d^2}, \tag{10}$$

where d is the distance between the centres of the two bubbles and κ is the compressibility of the bubble. Integrating from the initial distance between the bubbles d_0 to 0 yields the collision time

$$t_\mathrm{c} = -\int_{d_0}^{0} \frac{27\eta}{\left(2\pi\, f\, p_\mathrm{a}\right)^2 \rho\, \kappa^2\, R_0^5}\, d^2\, \mathrm{d}d = \frac{9\eta}{\left(2\pi\, f\, p_\mathrm{a}\right)^2 \rho\, \kappa^2} \frac{d_0^3}{R_0^5}. \tag{11}$$

In a standing wave field, bubbles with resonance frequencies higher than the transmitted sound field aggregate at the pressure antinodes, whereas bubbles with resonance frequencies lower than the transmitted sound field aggregate at the pressure nodes [13]. Hence, the ultimate distance d_∞ between clusters must be a quarter of the wavelength, *i.e.*,

$$d_\infty = \frac{\lambda}{4} = \frac{c}{4f}. \tag{12}$$

Both processes of bubble clusters aggregating and the movement of clusters in the direction of the sound field can be described by a simplified version of (5):

$$v = \frac{\mathrm{d}h}{\mathrm{d}t} \approx \frac{p_\mathrm{a}^2}{6\,\rho\, c\, f\, \eta} \frac{\delta\left(\dfrac{f_\mathrm{c}}{f}\right)}{\left[\left(\dfrac{f_\mathrm{c}}{f}\right)^2 - 1\right]^2 + \left[\delta\left(\dfrac{f_\mathrm{c}}{f}\right)\right]^2}\,, \tag{13}$$

where h is the distance travelled by the cluster and f_c is the cluster resonance frequency, for which $f_\mathrm{c} < f_0$ must hold, since the bubble cluster radius $R_\mathrm{c} > R_0$. For the bubble cluster compressibility κ_c, $\kappa \leq \kappa_\mathrm{c} < \kappa_\mathrm{f}$ must hold, in which κ_f is the compressibility of a free (unencapsulated) gas bubble.

Bubble coalescence is the fusion of two or more bubbles. As adjacent bubbles collide or expand, the pressure in the film between them increases, resulting in a deformation (flattening) of the bubble surfaces. The continuing bubble expansion causes drainage of the interposed film. This thinning continues until a critical thickness around $0.1\,\mu$m is reached, at which the Van der Waals attractive forces result in film rupture and the coalescence of the bubbles [16]. Film drainage is generally much faster for free (unencapsulated) bubbles than for encapsulated bubbles, as a result of the flow pattern in the draining film [17].

The coalescence mechanism of lipid-encapsulated microbubbles was investigated, based on high-speed optical observations of sonicated lipid-encapsulated ultrasound contrast agent microbubbles [17]. It was

found that, when sonicated at high acoustic amplitudes, lipid-encapsulated microbubbles expose free surfaces during the expansion phase, speeding up the coalescence process dramatically. Hence, for the formation of bubble clouds or microfoams, the use of low acoustic amplitudes is desirable.

3 Materials and Methods

A schematic overview of our experimental setup for simultaneous optical observations during sonication is shown in Figure 1. A polycarbonate container was built with internal dimensions: $24 \times 18 \times 15\,(\mathrm{cm})^3$. To give access to a microscope objective lens, a hole with an 11-mm diameter had been drilled in the base, covered with a 2-mm thick test slide (Jencons (Scientific) Ltd, Leighton Buzzard, Bedfordshire, UK). The container was filled with 2.6 L tap water. The container was placed on an $x-y$-table on top of a DM IRM inverted microscope (Leica Microsystems Wetzlar GmbH, Wetzlar, Germany) with two objective lenses: a 506075 C-Plan 10× objective lens (Leica Microsystems Wetzlar GmbH) with a 0.22 numerical aperture and a 506236 N-Plan 50× objective lens (Leica Microsystems Wetzlar GmbH) with a 0.50 numerical aperture. A Mille Luce$^{\mathrm{TM}}$ Fiber Optic Illuminator Model M1000 (StockerYale, Inc., Salem, NH, USA) was connected to an optic fibre with a 7-mm diameter leading into the water of the container. It was placed in line with the objective lens, as shown in Figure 2.

The charge couple device (CCD) of a FASTCAM MC1 high-speed camera (Photron (Europe) Limited, West Wycombe, Bucks, United Kingdom) was mounted to the microscope and connected to its processing unit, which was capable of recording images at 10,000 frames per second. The camera was controlled by a laptop computer.

3.1 Ultrasound

A laptop computer triggered a DATAMAN-530 arbitrary waveform generator (Dataman Programmers Ltd, Maiden Newton, Dorset, UK), which was connected to a 2100L 50-dB RF power amplifier (Electronics & Innovation Ltd., Rochester, NY, USA). The power amplifier was connected to an undamped broadband single element transducer containing a Pz37 Piezo crystal (Ferroperm Piezoceramics A/S, Kvistgård, Denmark) with a centre frequency of 2.2 MHz. The design of the transducer has been described in [18]. Transmitted signals were typically continuous with frequencies in the range 1-10 MHz. The peak-negative acoustic pressures were determined using a PVdF needle hydrophone system with a 0.2-mm probe (Precision Acoustics Ltd, Dorchester, Dorset, UK) connected to a TDS 420A oscilloscope (Tektronix, Inc., Beaverton, OR, USA).

The ultrasound transducer was positioned in the container using a clamp stand, at a focal distance of 38 mm from the region of interest to be studied. The azimuth of the length axis of the transducer relative to the North of the

container was 37° and the elevation of the length axis of the transducer relative to the base of the container was 17°, as shown in Figure 2.

3.2 Ultrasound contrast agent

DEFINITY® (Lantheus Medical Imaging, North Billerica, MA, USA) consists of C_3F_8 gas microbubbles with mean diameters between 1.1 and 3.3 μm, encapsulated by lipid/surfactant shells. Its resonance frequency had been measured to be 2.7 MHz [19]. The 1.5-ml vials used in our experiments had been stored at 9°C. Each vial was shaken for 45 s using a Vialmix® device (Lantheus Medical Imaging). Before introducing the ultrasound contrast agent in our setup, it was further diluted using a 0.9% saline solution.

The diluted ultrasound contrast agent was inserted using a syringe into a microbore tube with a 0.51-mm inner diameter. The tube led to a CUPROPHAN® RC55 cellulose capillary (Membrana GmbH, Wuppertal, Germany) with a 200-μm inner diameter and an 8-μm wall thickness. The middle of the capillary coincided with the optical focus of the objective lens and with the acoustic focus of the ultrasound transducer, as shown in Figure 2. The typical field of view using the 10× objective lens was $500 \times 200\,(\mu\mathrm{m})^2$, whereas the diameter of the acoustic focus was greater than 5 mm. Hence, the whole field of view could be considered in acoustic focus. The capillary was positioned 2 mm from the base of the container. The flow speed of the ultrasound contrast agent through the capillary was manually controlled.

In total, 48 experiments were performed. Bubble and cluster sizes were measured and tracked using Image-Pro Plus (Media Cybernetics, Inc., Bethesda, MD, USA). Further analysis was done using MATLAB® (The MathWorks, Inc., Natick, MA, USA).

4 Results and Discussion

At the high concentrations we used, clustering started instantaneously after the ultrasound generator was switched on. Figure 3 illustrates the speed of cluster formation of DEFINITY® ultrasound contrast agent that had been further diluted to 1:20. With distances between the microbubbles of only few micrometres, collision times from (11) should be within a second, indeed, as shown in Figure 4. Also, from (11) and Figure 4 it is explained why cluster formation must be faster at higher frequencies, if the other acoustic parameters and the concentration are not changed. Or, after a fixed duration, larger clusters must have formed using higher frequencies, since bubble can approach from larger d_0 at higher f. These deductions are confirmed by our experimental observations: In Figure 3, after 233 ms two clusters had been formed of approximately 15 μm each. These started to approach in the subsequent frames. Overall, newly-formed clusters collided to form larger clusters. This is illustrated by Figures 5 and 6. Each branch represents a cluster. The branches coming together represent the collision of clusters into larger clusters. The velocities of the clusters are on the order of tens of micrometres per second. Although increasing the acoustic pressure would increase the cluster velocities dramatically, as is evident from (13), they would also lead to microbubble disruption [14]. We did not observe phenomena associated with microbubble disruption.

The larger a cluster grows, the lower its resonance frequency becomes. Hence, the velocity of a cluster in the direction of the sound field, defined by (13), should decrease in time. If two identical clusters with resonance frequency f_0 merge, the resulting resonance frequency $f_\mathrm{c}' \approx \left(2^{-\frac{1}{3}}\right) f_0 = 0.79\, f_0$ [1]. Assuming that the compressibility and damping coefficient do not substantially change, a similar decrease in cluster velocity is expected. However, the decrease in slope magnitude of the main branch in Figure 5 is negligible. This might be explained if the resulting cluster is much stiffer than the original clusters, increasing the damping coefficient.

Also, 7 MHz must be further off the cluster resonance frequency than 2 MHz. Hence, the magnitudes of the slopes in Figure 6 are lower than those than in Figure 5. Secondary radiation forces of clusters onto each other do not explain the cluster colliding times observed. Even if the compressibility of the clusters would be equal to that of a single ultrasound contrast agent microbubble, under the acoustic conditions we used, the collision times from (11) would be just milliseconds. Hence, the bubble clusters cannot be regarded as identical monopoles in our setting. A close-up of two colliding clusters with 22-μm diameters forming a 25-μm cluster is shown in Figure 7. The total time spanning this process is slightly less than 1.8 s.

The clusters were initially formed in the middle of the capillary. These clusters were located at distances $d_0 < \frac{1}{4}\lambda$, as demonstrated in Figure 8. However, following further cluster coalescence during 17.55 seconds of sonication, the final distance between the larger clusters corresponded to $\frac{1}{4}\lambda = 54\,\mu$m. These had been pushed towards the lower capillary wall, owing to primary radiation forces.

The cluster velocities towards the capillary wall were between $5\,\mu\mathrm{m\,s^{-1}}$ at 7 MHz and 22 kPa peak-negative pressure and $15\,\mu\mathrm{m\,s^{-1}}$ at 2 MHz and 20 kPa peak-negative pressure sonication. These are of the same order as the left-hand side term in (13). The magnitudes of the slopes in Figure 6 did not change close to the capillary wall. Hence, in our experimental setup, we neglected any effect of the capillary wall on cluster translation. With cluster diameters less than $30\,\mu$m, buoyancy effects may neglected on our timescales as well.

In summary, we observed the following stages of microfoam formation, illustrated in Figure 9. Our initial situation was a dense, random bubble distribution before ultrasound arrival. After the sonication started, contrast microbubbles collided, owing to secondary radiation forces. Subsequently, these clusters coalesced within the space of a quarter of the wavelength, owing to primary radiation forces. The resulting microfoams translated in the direction of the ultrasound field, owing to primary radiation forces.

Small deviations in microbubble sizes or shell properties lead to deviations in individual bubbles's resonance frequencies, as expressed in (8). These in turn cause oscillation phase differences, as expressed in (6), big enough to be optically observed [7]. Therefore, predicting and manipulating individual microbubbles is technically challenging. We have demonstrated that as soon as the bubble clusters were formed and as long as they were in the sound field, they behaved as one entity. At our acoustic settings, it took seconds to force the bubble clusters to positions approximately $\frac{1}{4}\lambda$ apart. It also just took seconds to drive the clusters towards a boundary.

We may assume that vessel blocking can only be successful if a microfoam is created with a diameter equal to or greater than the vessel diameter d_v. From this study it follows that in order to create such a foam, $\frac{1}{4}\lambda > d_\mathrm{v}$, or, $f < \frac{c}{4\,d_\mathrm{v}}$.

For therapeutic purposes, it would be of great interest to induce microjetting on entire clusters towards a vessel wall, presumably causing sonoporation or sonolysis. Although ultrasound-induced microjetting has been observed with ultrasound contrast agents, its occurrence in *in vivo* situations is hard to control [20,21]. Predictable sonic manipulation would be better feasible if the microbubbles would be forced to clusters of known size and position first.

5 Conclusions

We observed the following stages of microfoam formation within a densely populated concentration of microbubbles. After the sonication started, contrast microbubbles collided, forming small clusters, owing to secondary radiation forces. These clusters coalesced within the space of a quarter of the ultrasonic wavelength, owing to primary radiation forces. The resulting microfoams translated in the direction of the ultrasound field, hitting the capillary wall, also owing to primary radiation forces.

We have demonstrated that as soon as the bubble clusters were formed and as long as they were in the sound field, they behaved as one entity. At our acoustic settings, it took seconds to force the bubble clusters to positions approximately a quarter wavelength apart. It also just took seconds to drive the clusters towards the capillary wall.

Subjecting ultrasound contrast agent microbubbles to a continuous low-amplitude signal makes them cluster to know positions and known microfoam sizes, allowing for straightforward sonic manipulation.

6 Acknowledgements

The authors are grateful to Lantheus Medical Imaging, North Billerica, MA, USA, for supplying the ultrasound contrast agent DEFINITY®. This work has been supported by DFG Emmy-Noether Programme grant 38355133, EPSRC grant EP/F037025/1 and the HERI Research Pump Priming Fund.

References

[1] M. Postema, G. Schmitz, Bubble dynamics involved in ultrasonic imaging, Expert Rev. Mol. Diagn. 6 (3) (2006) 493–502.

[2] J. R. Lindner, S. Kaul, Delivery of drugs with ultrasound, Echocardiography 18 (4) (2001) 329–337.

[3] E. C. Unger, T. O. Matsunaga, T. McCreery, P. Schumann, R. Sweitzer, R. Quigley, Therapeutic applications of microbubbles, Eur. J. Radiol. 42 (2002) 160–168.

[4] N. Kudo, T. Miyaoka, K. Okada, K. Yamamoto, K. Niwa, Study on mechanism of cell damage caused by microbubbles exposed to ultrasound, Proc. IEEE Ultrason. Symp. (2002) 1351–1354.

[5] M. Postema, O. H. Gilja, Ultrasound-directed drug delivery, Curr. Pharm. Biotechnol. 8 (6) (2007) 355–361.

[6] P. A. Dayton, J. S. Allen, K. W. Ferrara, The magnitude of radiation force on ultrasound contrast agents, J. Acoust. Soc. Am. 112 (5) (2002) 2183–2192.

[7] M. Postema, M. Mleczko, G. Schmitz, Mutual attraction of oscillating microbubbles, in: T. M. Buzug, D. Holz, S. Weber, J. Bongartz, M. Kohl-Bareis, U. Hartmann (Eds.) Advances in Medical Engineering, Springer, Berlin, 2007, vol. 19 of *Methods of experimental physics*, pp. 75–80.

[8] P. A. Dayton, K. E. Morgan, A. L. Klibanov, G. Brandenburger, K. R. Nightingale, K. W. Ferrara, A preliminary evaluation of the effects of primary and secondary radiation forces on acoustic contrast agents, IEEE Trans. Ultrason., Ferroelect., Freq. Contr. 44 (6) (1997) 1264–1277.

[9] P. Tortoli, V. Michelassi, M. Corsi, D. Righi, Y. Takeuchi, On the interaction between ultrasound and contrast agents during Doppler investigations, Ultrasound Med. Biol. 27 (9) (2001) 1265–1273.

[10] H. Medwin, Counting bubbles acoustically: a review, Ultrasonics 15 (1977) 7–13.

[11] J. Magnaudet, I. Eames, The motion of high-Reynolds-number bubbles in inhomogeneous flows, Annu. Rev. Fluid Mech. 32 (2000) 659–708.

[12] P. Di Marco, W. Grassi, G. Memoli, Experimental study on rising velocity of nitrogen bubbles in FC-72, Int. J. Therm. Sci. 42 (2003) 435–446.

[13] T. G. Leighton, The Acoustic Bubble, Academic Press Ltd, London, 1994.

[14] M. Postema, G. Schmitz, Ultrasonic bubble in medicine: influence of the shell, Ultrason. Sonochem. 14 (4) (2007) 438–444.

[15] N. de Jong, R. Cornet, C. T. Lancée, Higher harmonics of vibrating gas-filled microspheres. Part one: simulations, Ultrasonics 32 (6) (1994) 447–453.

[16] P. C. Duiveveld, Bouncing and coalescence of two bubbles in water, sine nomine, Sine loco, 1994.

[17] M. Postema, P. Marmottant, C. T. Lancée, S. Hilgenfeldt, N. de Jong, Ultrasound-induced microbubble coalescence, Ultrasound Med. Biol. 30 (10) (2004) 1337–1344.

[18] S. Kotopoulis, A. Schommartz, M. Postema, Sonic cracking of blue-green algae, Appl. Acoust. 70 (10) (2009) 1306–1312.

[19] E. Kimmel, B. Krasovitski, A. Hoogi, D. Razansky, D. Adam, Subharmonic responce of encapsulated microbubbles: condition for existance and amplification, Ultrasound Med. Biol. 33 (11) (2007) 1767–1776.

[20] M. Postema, A. van Wamel, F. J. ten Cate, N. de Jong, High-speed photography during ultrasound illustrates potential therapeutic applications of microbubbles, Med. Phys. 32 (12) (2005) 3707–3711.

[21] P. Prentice, A. Cuschieri, K. Dholakia, M. Prausnitz, P. Campbell, Membrane disruption by optically controlled microbubble cavitation, Nature Phys. 1 (2005) 107–110.

List of Figures

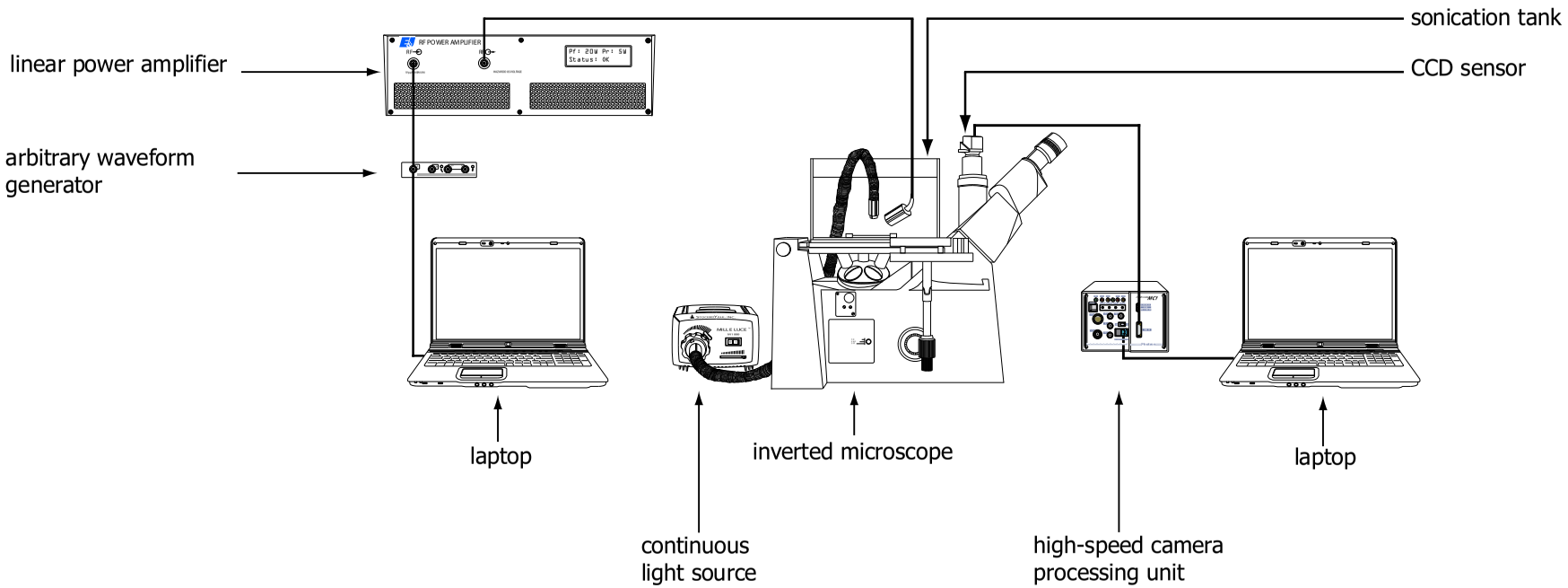

Fig. 1. Schematic overview of the experimental setup

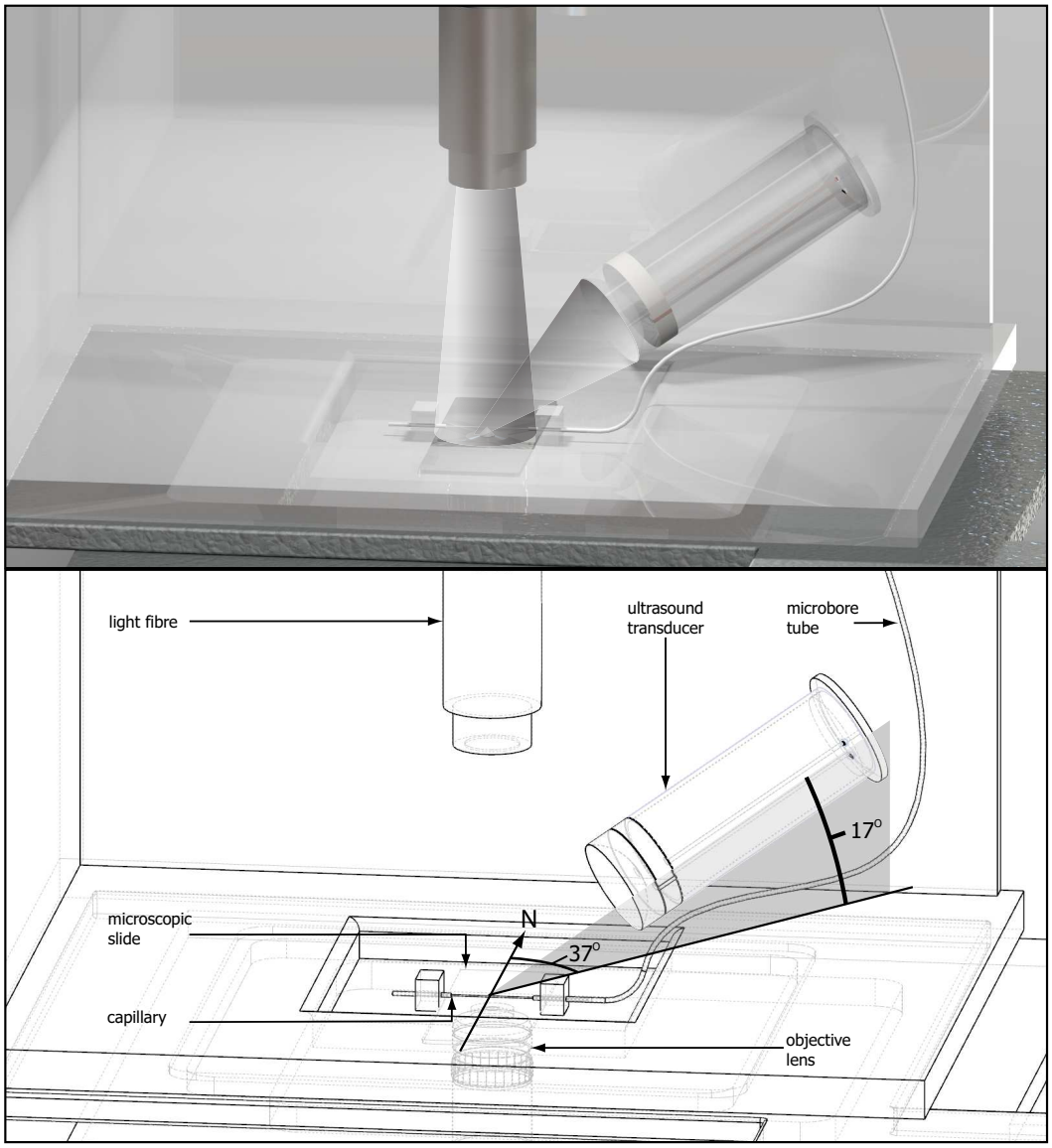

Fig. 2. Close-up of the sonication tank with coinciding sound, light beam, and objective focus *(top)* and definitions of the azimuth and elevation of the transducer relative to the North of the container *(bottom)*.

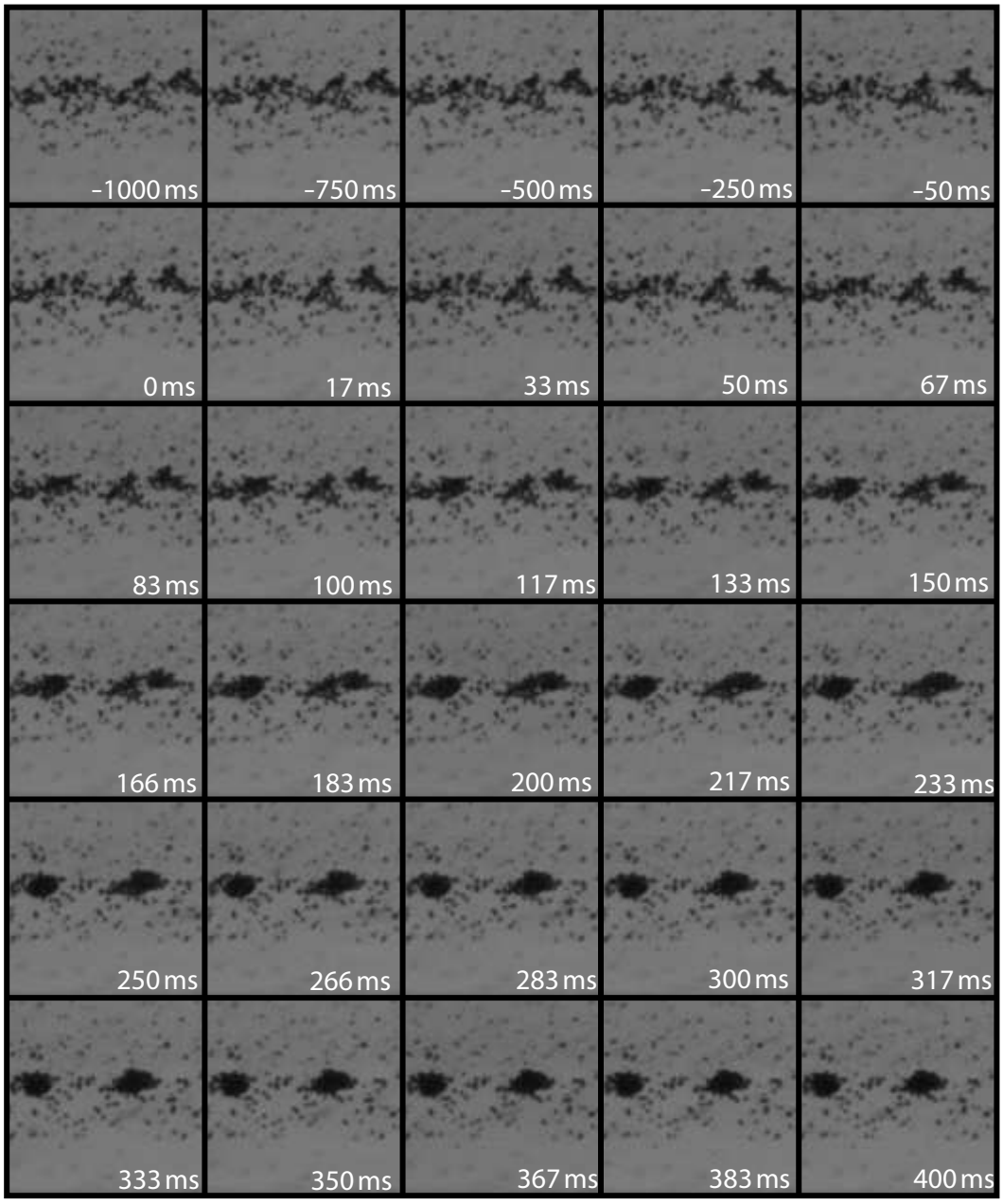

Fig. 3. Microfoam formation during continuous sonication at 2 MHz and 20 kPa peak-negative acoustic pressure. Each frame corresponds to a $120 \times 120\,(\mu\mathrm{m})^2$ area. Time $t = 0$ was defined by the start of the sonication.

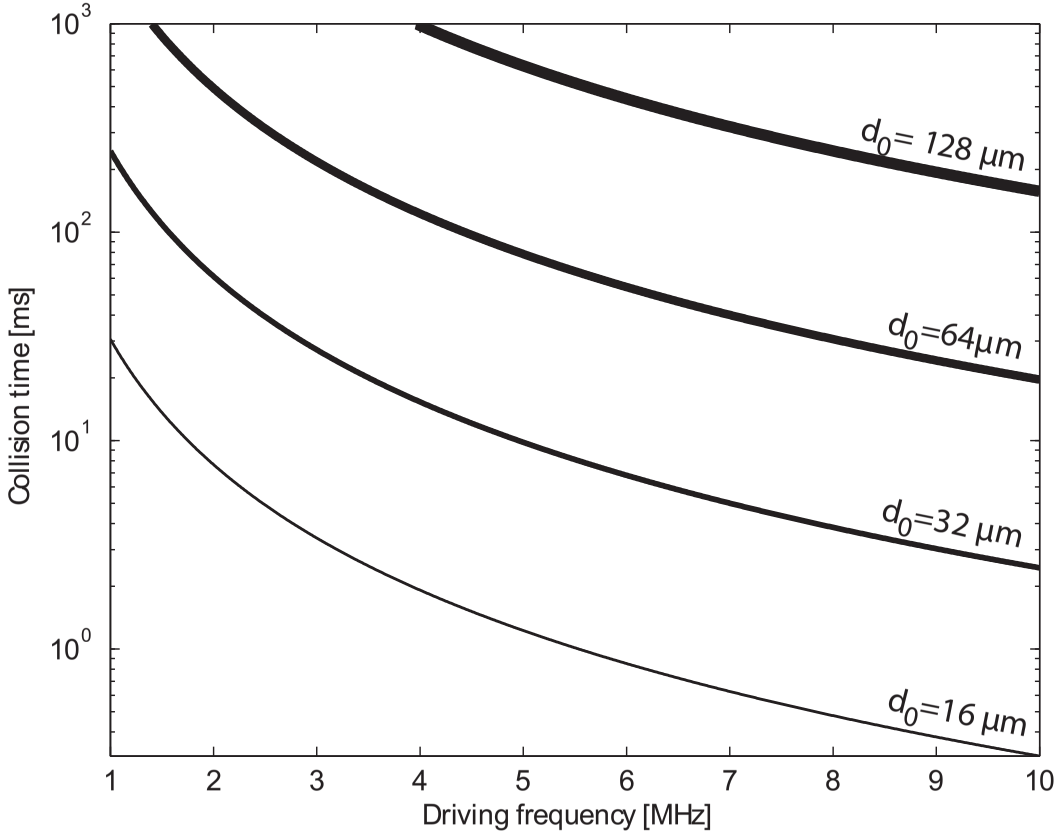

Fig. 4. Collision times of individual encapsulated microbubbles as a function of driving frequency at given distances d_0, using $p_\mathrm{a} = 20\,\mathrm{kPa}$, $R_0 = 1.25\,\mu\mathrm{m}$, $\kappa = 5 \times 10^{-6}\,\mathrm{m^2\,N^{-1}}$, and $\rho = 998\,\mathrm{kg\,m^{-3}}$.

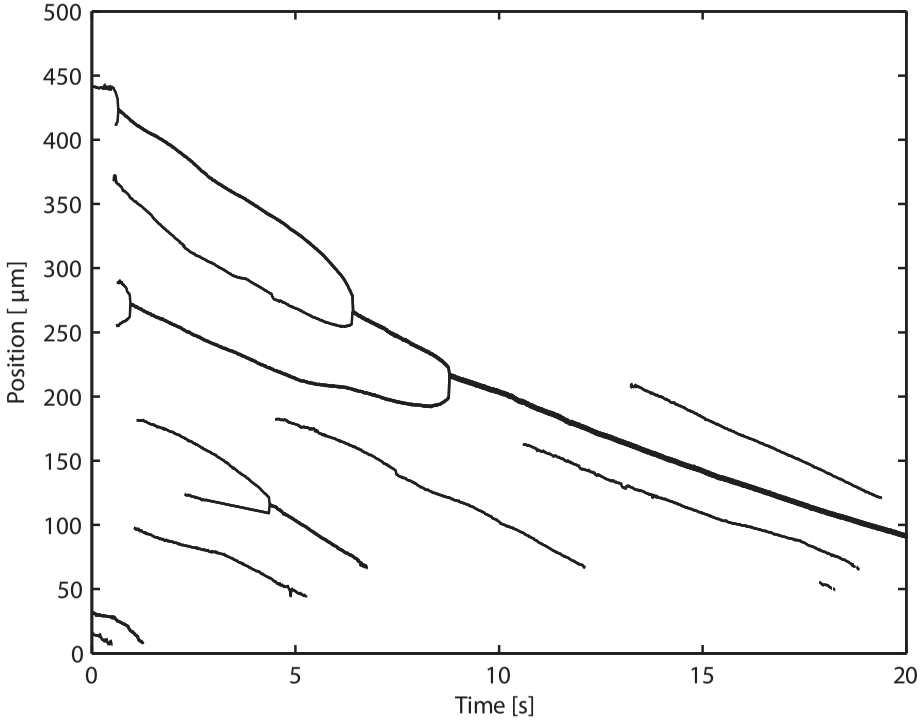

Fig. 5. Cluster positions as a function of time, during continuous sonication at 2 MHz and 20 kPa peak-negative acoustic pressure. Position in the capillary is defined from East (0 μm) to West (500 μm). Bold lines indicate merged clusters. The beginning *(left)* of a line indicates the formation of a cluster of diameter $> 6.8\,\mu$m. The end *(right)* of a line indicates the disintegration or contraction of a cluster to a diameter $< 6.8\,\mu$m.

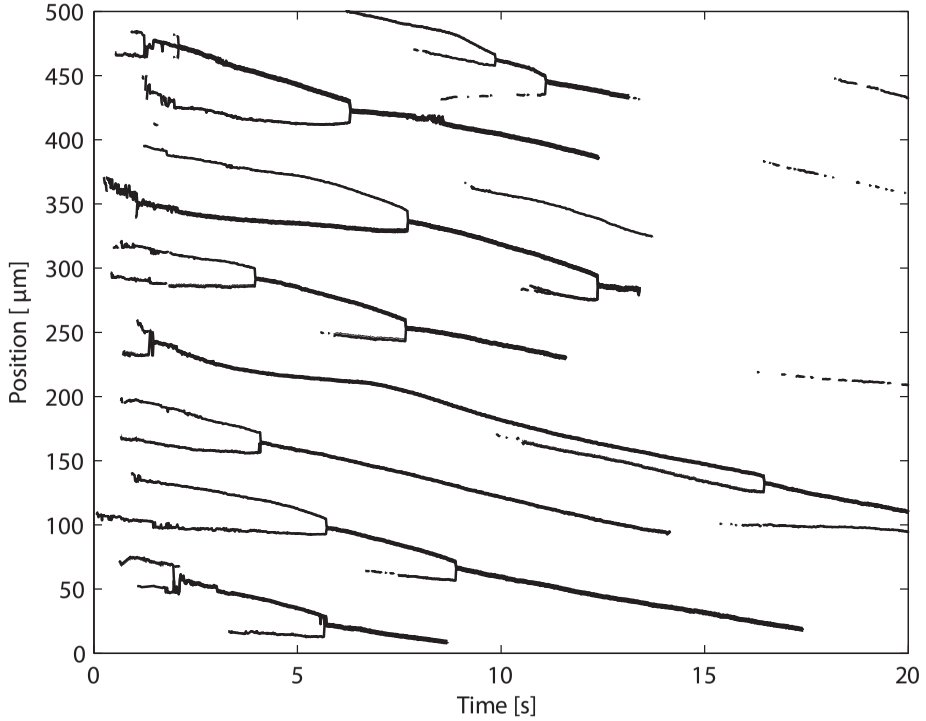

Fig. 6. Cluster positions as a function of time, during continuous sonication at 7 MHz and 22 kPa peak-negative acoustic pressure. Position in the capillary is defined from East (0 μm) to West (500 μm). Bold lines indicate merged clusters. The beginning *(left)* of a line indicates the formation of a cluster of diameter $> 6.8\,\mu$m. The end *(right)* of a line indicates the disintegration or contraction of a cluster to a diameter $< 6.8\,\mu$m.

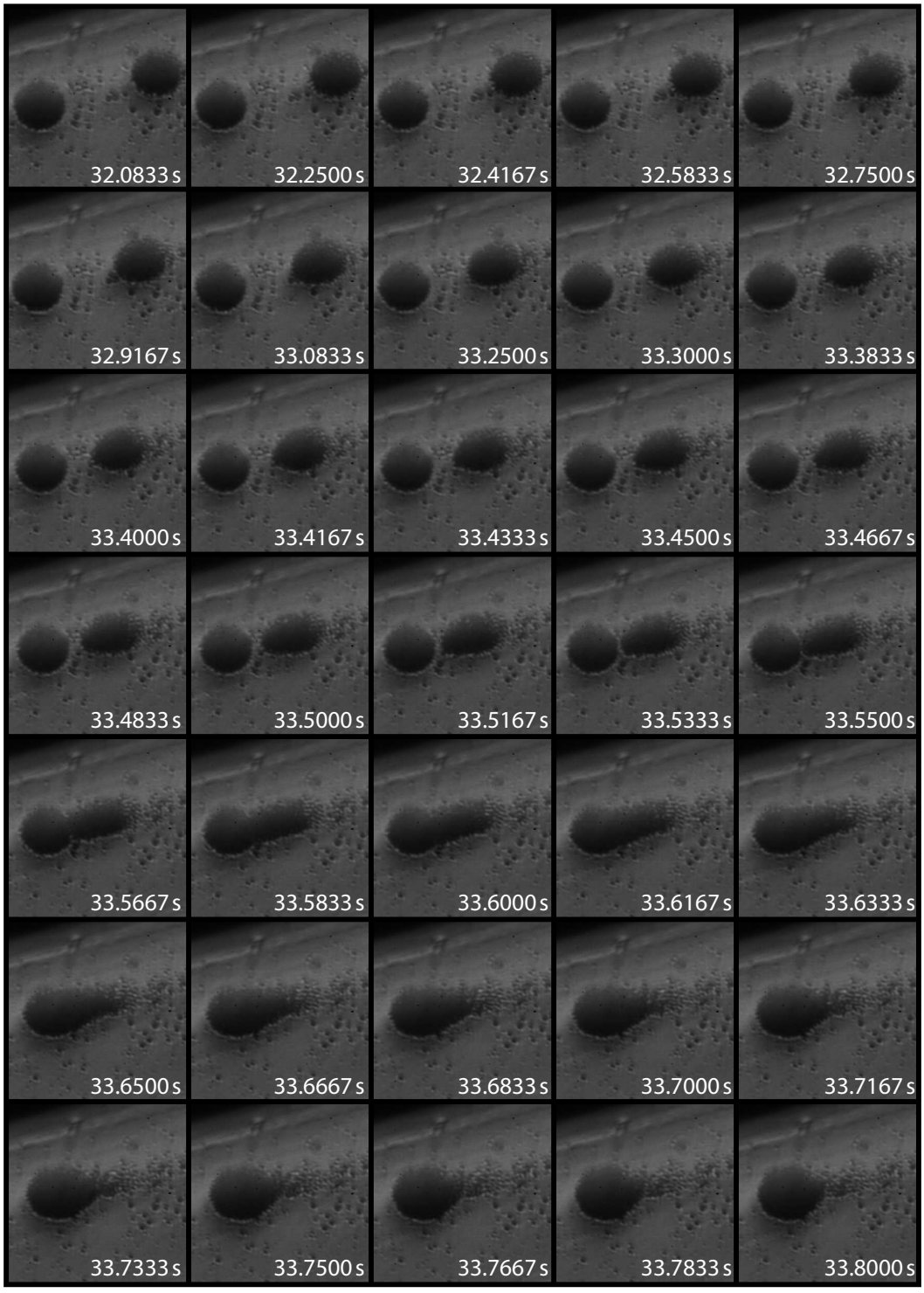

Fig. 7. Two clusters, with 22-μm diameters and an initial distance of 55 μm, colliding and coalescing during continuous sonication at a 2-MHz driving frequency and a 20-kPa peak-negative pressure. The frame size corresponds to 81×81 $(\mu\text{m})^2$. Times were relative to the start of the sonication *(t=0)*.

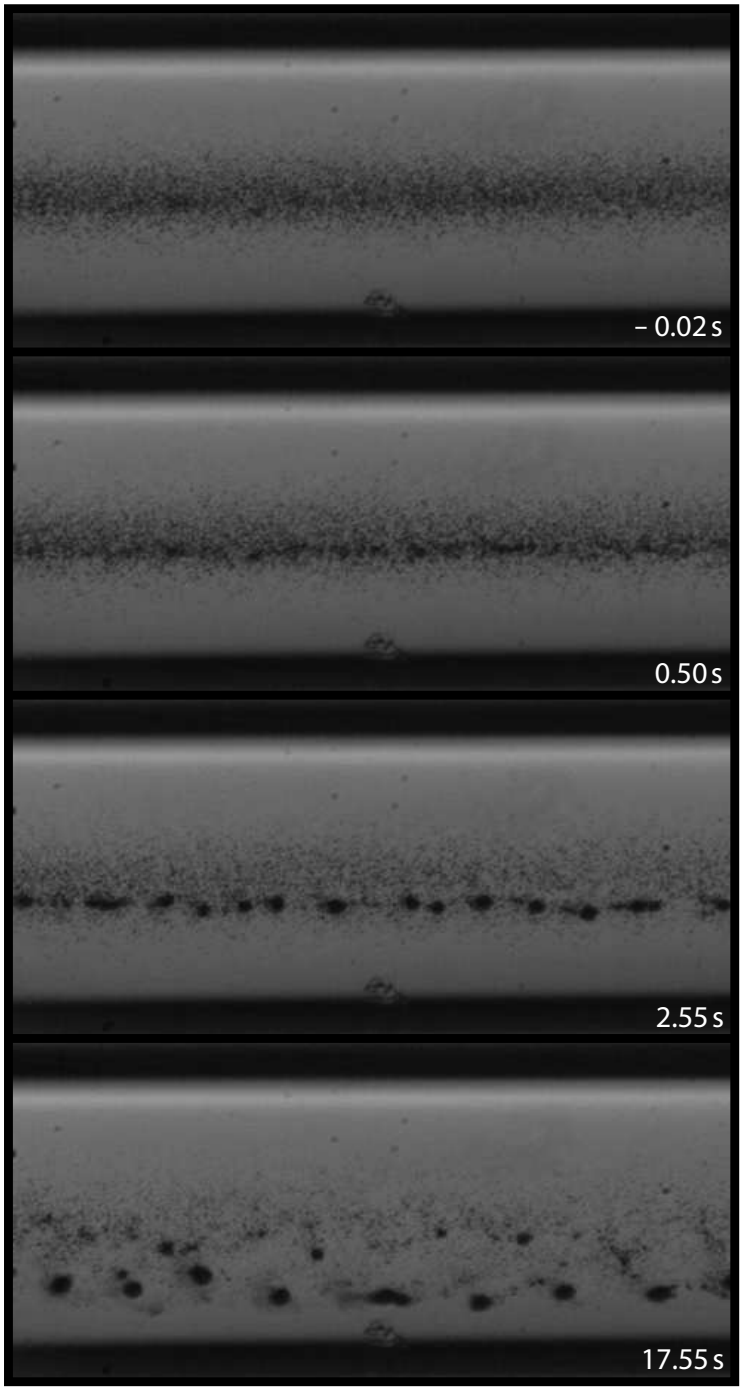

Fig. 8. Clusters forming during sonication at 7 MHz and 22 kPa peak-negative pressure. The frame size corresponds to $560 \times 264\,(\mu\mathrm{m})^2$. Time $t = 0$ was defined by the start of the sonication.

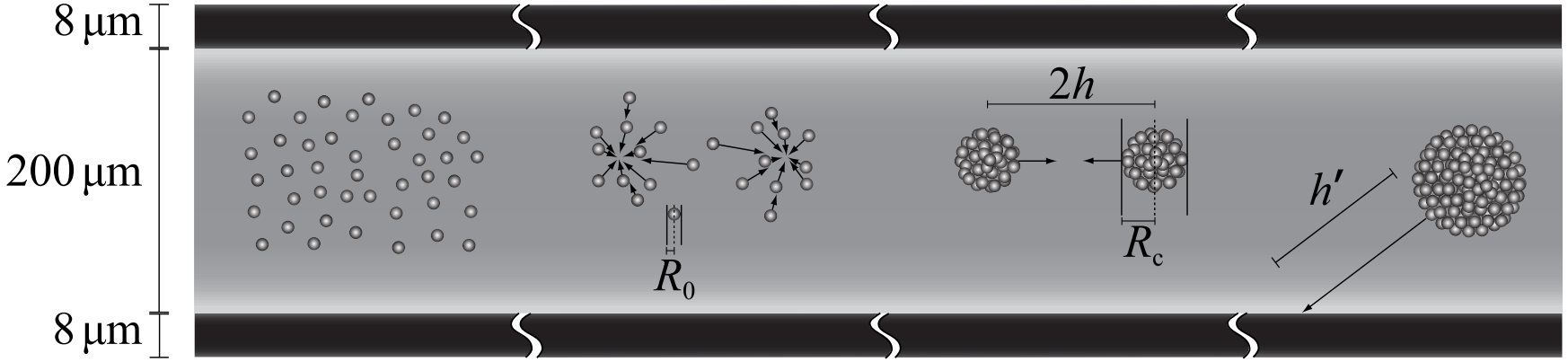

Fig. 9. Schematic representation of the four stages of microfoam formation in a capillary: *(left–right)* random bubble distribution before ultrasound arrival, bubbles colliding during sonication, cluster coalescing within the space of a quarter of the wavelength, microfoam translation.